Vol. 86 (1994) *ACTA PHYSICA POLONICA A* No. 4

Proceedings of the ISSSRNS '94, Jaszowiec 1994

CHARACTERIZATION OF CONCAVE-CURVED SPECTROMETERS FOR 2D X-RAY OPTICS

F.N. Chukhovskii, W.Z. Chang and E. Förster

X-Ray Optics Group of the Max-Planck-Gesellschaft
at the Friedrich-Schiller University of Jena, 07743 Jena, Germany

A procedure for calculating X-ray intensity profiles analytically for various X-ray diffraction geometries has been developed, which takes into account the misalignment, the solid angle factor, the effects of convergence and/or divergence of the diffracted X-rays. The approach is applicable to X-ray optics with either a point source or a quasi-parallel beam. Moreover, using this procedure allows one to calculate the magnified image from a plasma source, the intensity profiles of topographs of bent crystals, and the spectral resolution of various focusing geometries. Several examples are presented to demonstrate the applications of this procedure. Using non-dispersive and dispersive double-crystal spectrometers, rocking curves were measured for singly and doubly bent crystals. The agreement was satisfactory with the X-ray dynamic theory of bent crystals. Furthermore, we have also extended the study of X-ray optics to include the crystal anisotropic effects. The anisotropic elasticity theory is applied to bend crystals for calculating the diffracting region on the crystal surface. The anticlastic curvature effects are analytically demonstrated with respect to the crystals' diffracting area.

PACS numbers: 07.85.+n, 29.30.Kv

1. Introduction

Curved diffractors for imaging and focusing X-rays are of great interest in X-ray optics and their applications in X-ray spectroscopy, X-ray imaging, and X-ray plasma diagnostics [1–3]. Hence, it is necessary to be able to evaluate X-ray optical systems by employing curved diffractors in order to optimize a given system's performance. A procedure for calculating X-ray intensity profiles analytically for various X-ray diffraction geometries has been developed [2], which takes into account the misalignment, the solid angle factor, the effects of convergence and/or divergence of the diffracted X-rays. The method is versatile to X-ray optics with either a point source or a quasi-parallel beam. In this article, several examples to plasma imaging, to synchrotron radiation source, and to measurement of the bent crystals' parameters are illustrated.

Both non-dispersive and dispersive arrangement of the double-crystal spectrometer for measuring the rocking curves of bent crystals are presented [4–5]. The

experimental results are compared with the theoretical calculations which include the reflection curve of the bent crystal described by Takagi–Taupin theory and the effect of the finite source size.

Moreover, the investigation to the crystal anisotropic effects on bent crystal X-ray optics has also been performed [6]. The anisotropic elasticity theory is applied to bent crystals for calculating the diffracting region on the crystal surface. The relationship of the radii of curvature for bent crystals and the crystal compliance tensor is obtained. The anticlastic curvature effects are analytically shown with respect to the diffracting area and the collection solid angle. It is illustrated that the occurrence of the anticlastic curvature effect directly depends on the crystal orientation.

2. Calculations of X-ray intensity profiles for various diffraction geometries

For the calculation several assumptions have been made as the following: (1) the source is an ideal point source; (2) the diffractor (curved crystal) size is small compared with the radius of the focal circle; and (3) the crystal rocking curve is a Gaussian distribution. The last assumption implies that the crystal's rocking curve can be expressed as follows:

$$R(\Delta\theta) = I/I_0 = \exp(-\Delta\theta^2/\Delta\theta_0^2 \ln 2), \tag{1}$$

where $\Delta\theta_0$ is half the full width at half maximum for the rocking curve, and $\Delta\theta$ is the angular deviation; I and I_0 are the diffracted and incident intensities for a parallel beam; and R is the reflection coefficient. For a given diffraction geometry, shown in Fig. 1, with a curved diffractor, the intensity profile can be expressed in linear coordinates relative to the diffractor's surface by using relationships between $\Delta\theta$ and the linear coordinates. Then, the results of including the misalignment effects yield

$$\Delta\theta(x,z) = Ax^2+Bx^3+Cz^2+Dxz^2+Exz+Fx+Gz+Ix^2z+Jz^3+H, \tag{2}$$

where coefficients A through H containing the Bragg angle θ_B and misalignment parameters x_s, y_s, and z_s, are listed in Table I. For X-rays divergent from a point source, the diffracting region on the curved diffractor's surface subtends a solid angle $\Omega(x,z)$ at the source. The solid angle is expressed as a function of the Bragg angle and the misalignment parameters. The resulting reflection coefficient yields

$$R(x,z) = \exp[-\Delta\theta(x,z)^2/\Delta\theta_0^2 \ln 2]\Omega(x,z), \tag{3}$$

where Ω, the solid angle factor per unit surface area, is expressed as

$$\Omega(x,z) = \frac{\boldsymbol{PS}\cdot\boldsymbol{n}}{|\boldsymbol{PS}|^3|\boldsymbol{n}|}\left[\sqrt{\left(\frac{\partial y}{\partial x}\right)^2+\left(\frac{\partial y}{\partial z}\right)^2+1}\right]. \tag{4}$$

Equation (3) describes the intensity distribution on the surface of the curved crystal for either the aligned or misaligned case for a given point X-ray source. $\boldsymbol{PS}$ and $\boldsymbol{n}$ are the incident X-ray and the normal vectors, respectively (Fig. 1). The solid angle factor is needed for cases where the shape of the intensity distribution either on the surface or on the image plane is important due to the varying distances

TABLE I

Coefficients of Eq. (2).

$$\Delta\theta = Ax^2 + Bx^3 + Cz^2 + Dxz^2 + Exz + Fx + Gz + Ix^2Z + Jz^3 + H$$

$$A = \frac{1}{2\cos\theta_B}\left\{\frac{3m^2n}{K^{5/2}} - \frac{1}{K^{3/2}}\left[2m^2 + n\left(1 - \frac{n}{R_1}\right)\right] + \frac{1}{K^{1/2}}\left[2 - n - \frac{1}{R_1}\right]\right\}$$

$$B = \frac{1}{2\cos\theta_B}\left\{\frac{5m^3n}{K^{7/2}} - \frac{3m}{K^{5/2}}\left[m^2 + n(1 - \frac{n}{R_1})\right]\right.$$
$$\left. + \frac{m}{K^{3/2}}\left[3 - n - \frac{1+n}{R_1}\right] + \frac{m}{K^{1/2}}(1 - \frac{1}{R_1})\right\}$$

$$C = \frac{1}{2\cos\theta_B}\left\{\frac{3\zeta^2 n}{K^{5/2}} - \frac{1}{K^{3/2}}\left[\frac{2\zeta^2}{R_2'} + n\left(1 - \frac{n}{R_2}\right)\right] + \frac{1}{K^{1/2}}\left[\frac{2-n/R_2'}{R_2'} - \frac{1}{R_2}\right]\right\}$$

$$D = \frac{1}{2\cos\theta_B}\left\{\frac{15\zeta^2 nm}{K^{7/2}} - \frac{3m}{K^{5/2}}\left[\zeta^2\left(1 + \frac{1}{R_2'}\right) + n\left(1 - \frac{n}{R_2}\right)\right]\right.$$
$$\left. + \frac{m}{K^{3/2}}\left(\frac{2-n/R_2'}{R_2'} + 1 - \frac{1+n}{R_2}\right) - \frac{m}{K^{1/2}}\left(-\frac{1}{R_2'} - \frac{1}{R_2}\right)\right\}$$

$$E = \frac{m\zeta}{\cos\theta_B}\left[\frac{3n}{K^{5/2}} - \frac{1}{K^{3/2}}\left(1 + \frac{1}{R_2'}\right)\right]$$

$$F = \frac{m}{\cos\theta_B}\left(\frac{n}{K^{3/2}} - \frac{1}{K^{1/2}}\right)$$

$$G = \frac{\zeta}{\cos\theta_B}\left(\frac{n}{K^{3/2}} - \frac{1}{R_2' k^{1/2}}\right)$$

$$I = \frac{\zeta}{2\cos\theta_B}\left\{\frac{15m^2n}{K^{7/2}} - \frac{3}{K^{5/2}}\left(2m^2 + \frac{m^2}{R_2'} + 1 - \frac{n}{R_1}\right)\right.$$
$$\left. + \frac{1}{K^{3/2}}\left(1 + \frac{1}{R_2'}\right)\left(1 - \frac{n}{R_1}\right) + \frac{1}{R_2' K^{1/2}}(1 - \frac{1}{R_1})\right\}$$

$$J = \frac{\zeta}{2\cos\theta_B}\left\{\frac{5\zeta^2 n}{K^{7/2}} - \frac{3}{K^{5/2}}\left[\frac{\zeta^2}{R_2'} + n\left(1 - \frac{n}{R_2}\right)\right]\right.$$
$$\left. + \frac{1}{K^{3/2}}\left[\frac{3}{R_2'} - \frac{n}{2}\left(\frac{2}{(R_2')^2} - \frac{1}{R_2} - \frac{1}{R_2'}\right) - \frac{1+n/R_2'}{R_2} + \frac{1}{R_2' K^{1/2}}\left(\frac{1}{R_2'} - \frac{1}{R_2}\right)\right]\right.$$

$$H = -\tan\theta_B + \frac{n}{\cos\theta_B K^{1/2}}$$

R_1, R_2 = Radius of the surface || and $\perp$ to the focal circle plane,

R_1', R_2' = Radius of the planes || and $\perp$ to the focal circle plane,

$n = \sin^2\theta_B - y_s$, $m = x_s + \cos\theta_B \sin\theta_B$, x_s, y_s, and ζ are source displacements,

$K = x_s^2 + y_s^2 + z_s^2 + \sin^2\theta_B(1 - y_s) + 2x_s \sin\theta_B \cos\theta_B$.

In Table I $\zeta = z_s$

TABLE II

Various bent crystal diffraction geometries.

	R_1	R_2	R_2'
Johann	1	∞	∞
Johansson	1/2	∞	∞
Von Hamos	∞	1	1
Spherical	1	1	1
Toroidal	1	$\sin^2\theta_B$	$\sin^2\theta_B$

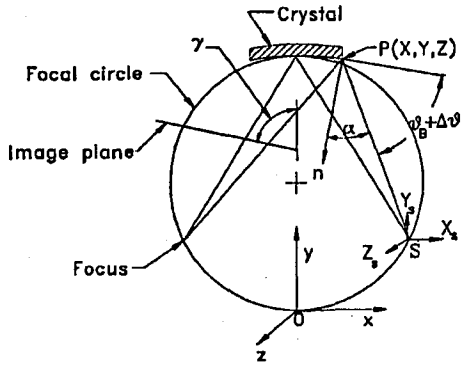

Fig. 1. Schematic diagram of the focal circle of a curved crystal diffractor. Coordinates of x_s, y_s, and z_s are parameters of the source position for possible misalignment. The coordinates used here are normalized by dividing the actual Cartesian coordinates by the crystal's radius of curvature.

between the diffractor surface and the source. For the intensity distribution of the diffracted X-rays at an arbitrary plane above, below, or at the focus can be obtained by projecting each point on the surface, which satisfies Eq. (3), onto the plane of interest.

Equation (2) can be applied to various diffraction geometries by setting the values of the normalized radius of curvature as shown in Table II. Thus, for a given geometry, $\Delta\theta$ is determined and so does the intensity profile on the surface of the crystal. Figure 2 illustrates intensity profiles for Johann, Johansson, von Hamos, and spherically bent crystal focusing geometries. It can be seen that for a given rocking curve width, Johann and Johansson geometries are nearly the same as far as the area of the surface used for diffraction. Certainly, Johansson will be more superior when the crystal size becomes larger in x direction. Clearly, there is nearly no difference of the intensity profiles for spherical and von Hamos geometries, which implies that the spherically bent crystal has no advantage of utilizing large diffraction area of the surface, but providing a quasi-focused diffracted beam in both x and z directions.

Moreover, the parameters, x_s, y_s, and z_s shown in Fig. 1 as a source displacement, can also be well applied to different cases:

(1) For imaging an X-ray plasma source, for example, x_s, y_s, and z_s can be selected for different values to obtain various magnifications of the source, e.g. $x_s < 0$ and $y_s > 0$. For obtaining a magnified (5×) image of the source, the spherically bent crystal used for imaging the X-ray plasma source is displaced from its aligned position, namely, the source is located closer to the crystal along the line joining the source and the center of the crystal shown in Fig. 3a. Using Eq. (3), an intensity profile over the surface of the crystal for a displaced point source is obtained, and shown in Fig. 3b. It is evident that only a small diffraction region of crystal is utilized to increase the spatial resolution and the desired magnification on the expense of losing collection efficiency of incident X-rays.

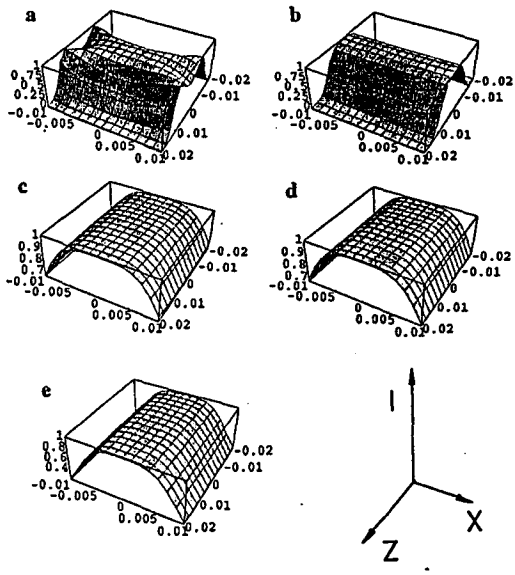

Fig. 2. Intensity profiles on the crystal surface for Johann case (a), Johansson case (b), spherically bent case (c), toroidally bent case (d) and von Hamos case (e). The Bragg angle used is 39.64° and the rocking curve width is 10^{-4} radian. x and z are normalized coordinates.

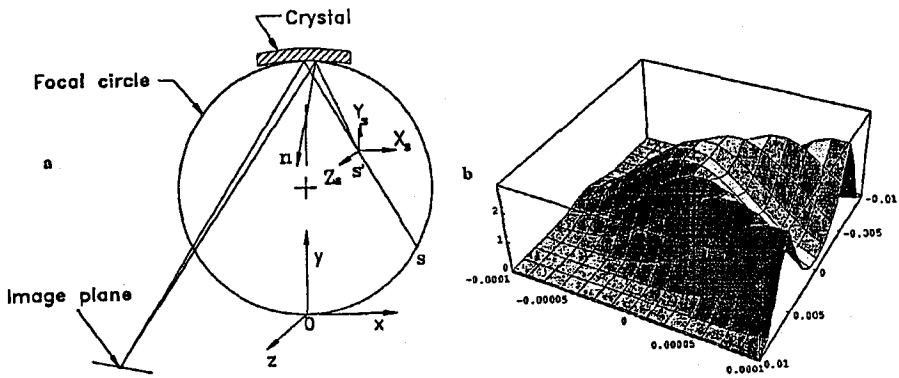

Fig. 3. (a) Schematic diagram of the focal circle of a curved crystal diffractor for a misaligned source position. The source is moved closer to the crystal surface along the line joining the source and the center point of the crystal. The amount displaced is $x_s = -d_1 \cos\theta_B$ and $y_s = d_1 \sin\theta_B$, where d_1 is the distance between s and s'. The magnification can be obtained by moving the source closer to the crystal. (b) Intensity profile on the surface of a spherically bent crystal with the Bragg angle 82.89°, rocking curve width 10^{-4}, radius of curvature 151 mm, and d_1 is 60.4 mm. Note that the scale of z is 100 times larger than that of x.

(2) For evaluating bent crystals' parameters, x_s, y_s, and z_s are used as fitting parameters to simulate the photographically recorded line profiles, so that the rocking curve width and the peak reflectivity of a crystal can be deduced. It should be noted that the rocking curve width of common diffraction crystals, as is generally known, is of the order of 10^{-5} to 10^{-3} radian. This is a rather small quantity to measure, and requires the divergent beam incident on the bent crystal to be confined to an angular range of no less than an order of 10^{-4}, which results an impractical incident intensity on the crystal surface. Figure 4 shows the difference in widths of two intensity profiles. Using the same Bragg angle and $\Delta\theta_0$, the half width of the rocking curve, Fig. 4a illustrates an intensity profile in angular units, whereas Fig. 4b shows the same profile in linear normalized coordinates along the x-axis. Due to the drastic difference in terms of their widths, it is evident that the intensity profile from Fig. 1b allows one to measure the actual width of the profile. This is, in fact, the key enabling one to measure the small quantity $\Delta\theta_0$ for bent crystals.

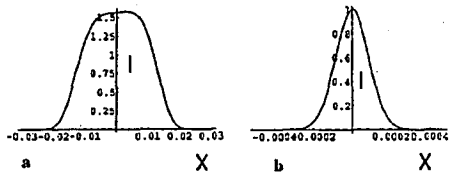

Fig. 4. Intensity line profile parallel to x-axis for (a) a cylindrically bent crystal, (b) a flat crystal. The Bragg angle used is 39.64° and the rocking curve width, $\Delta\theta_0 = 10^{-4}$.

By using a point X-ray source and the Johann diffraction geometry (Fig. 1), a topograph of the bent crystal can be obtained. The line profile across from the topograph, the intensity distribution is calculated using Eqs. (3) and (4) taking into account the effects of the crystal misalignment (x_s, y_s, and z_s), source broadening and wavelength spread of the X-ray emission line. The simulation continues until the calculated line profile matches the one obtained from the topograph. As a result, the rocking curve width $\Delta\theta_0$ the peak reflectivity and the status of the crystal alignment are known. Figure 5 illustrates the comparison of the experimental result and the simulation for a cylindrically bent mica crystal with Ti K_α radiation. This method has been proven to be unique for measuring the bent crystal parameters with a divergent beam from a point X-ray source.

(3) Furthermore, values of x_s, y_s, and z_s can be chosen such that the source is extended along the line joining the source and the mid-point of the diffractor's surface in a direction away from the focal circle (Fig. 1) then X-rays from this displaced source will reach the diffractor's surface with relatively small divergence in both meridional and sagittal directions. The degree of divergence is determined by the magnitude of the displacement of the source away from the focal circle. This suggests that Eqs. (1–3) can also describe the X-ray diffraction geometries with a synchrotron radiation source.

Figure 6 shows the configuration for the application to the synchrotron

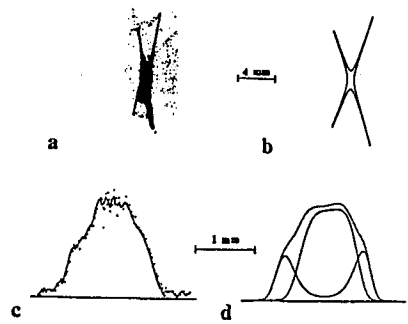

Fig. 5. Comparison of experimental and theoretical results for a mica diffractor of the Johann geometry: (a) topograph obtained with Ti K_α radiation; (b) calculated topograph based on $\Delta\theta_0 = \pm 9.95 \times 10^{-4}$; (c) measured intensity profile through the center of the topograph parallel to the x-axis; (d) calculated intensity profile which is the sum of K_{α_2} line (with two peaks) and K_{α_1} line (with one peak).

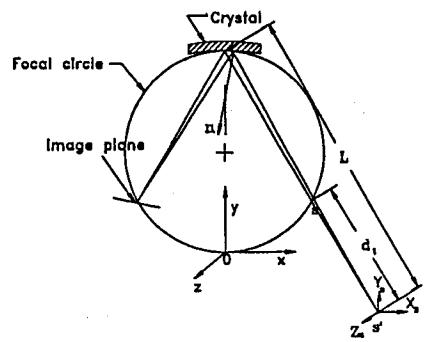

Fig. 6. Schematic diagram of a displaced virtual point source for quasi-parallel beam geometry. $x_s = d_1 \cos\theta_B$ and $y_s = -d_1 \sin\theta_B$, where d_1 is the distance between s and s'. The value of d_1 is determined by the divergence of the quasi-parallel beam for a given radius of curvature of the bent crystal.

source, where a cylindrically bent crystal is considered with the radius of curvature being a variable. The parameters x_s and y_s, in this case, equal $d_1 \cos\theta_B$ and $d_1 \sin\theta_B$, respectively and d_1 can be expressed in terms of the radius of curvature of the crystal R and the distance L,

$$d_1 = \frac{L}{2R} - \sin\theta_B. \tag{5}$$

For a given radiation, and a rocking curve width, the intensity profile on the surface of the crystal can be calculated by using Eq. (1) with various values of d_1. Several line profiles along the direction of x ($z = 0$) are calculated and shown in Figs. 7a and 7b. It can be seen that line profiles become wider, and they split into peaks as

d_1 increase from 0.001 to 0.01. The trend continues until the other peak vanishes, (outside the crystal region of interest), and the remaining peak becomes narrower. Figure 7b shows line profiles in a smaller scale, which exhibits continuing decrease in width of the profile until values of d_1 become larger than 1, which suggests, from this point, that the profile width will decrease to a finite value when the source is located further from the crystal.

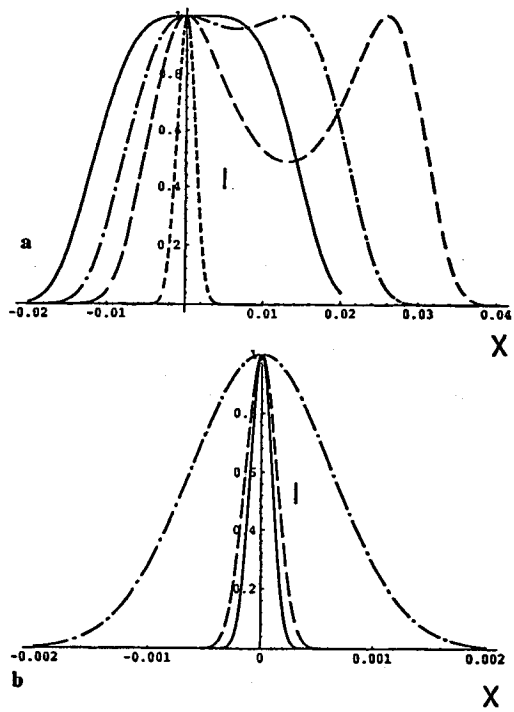

Fig. 7. Intensity line profiles on a cylindrically bent crystal for different values of d_1. The Bragg angle is 39.64° and $\Delta\theta_0 = 10^{-4}$. (a) $d_1 = 0.001$ for solid line, $d_1 = 0.005$ for dot-dashed line, $d_1 = 0.01$ for long dashed line, and $d_1 = 0.05$ for short dashed line. (b) $d_1 = 0.1$ for dot-dashed line, $d_1 = 0.5$ for dashed line, and $d_1 = 1$ for solid line. Note that the scale of (a) is 10 times larger than that of (b).

Figure 8 also illustrates the intensity profiles on the surface of the bent crystal. The radiation used here is 3.1 keV, the Bragg angle — 39.64°, and the width of the rocking curve — 10^{-4}. As it is expected when the value d_1 is 10^{-3}, the profile is nearly the same as in the case of the point source. When d_1 becomes larger, the profile curves to negative x direction, and the width becomes narrower, whereas the width wider in z direction. As a result, only a narrow portion of the crystal in x direction contributes to diffracting X-rays. Clearly, for a given distance between the crystal and the source, the radius of curvature can be varied in order to optimize for certain application. If the higher spatial resolution is desirable,

then the radius of curvature needs to be small, so that the displacement d_1 is large (Figs. 8c and d). On the other hand, if the intensity of diffracted beam is the major consideration, then the radius of curvature should be large and selected in such a way that d_1 tends to zero (Figs. 8a and b).

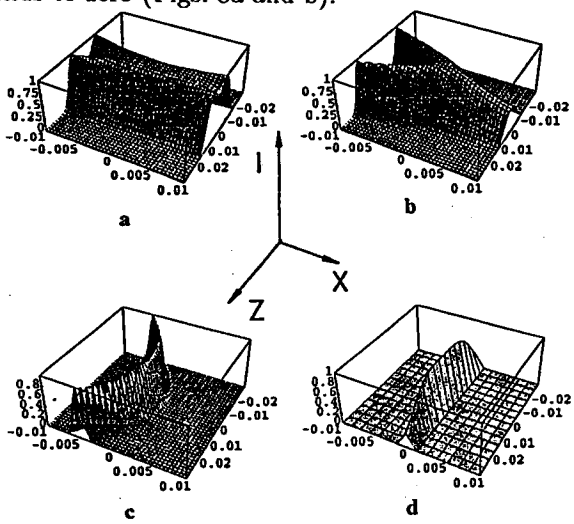

Fig. 8. Intensity profiles on the surface of a cylindrically bent crystal with the same parameters as in Fig. 7 for (a) $d_1 = 0.001$, (b) $d_1 = 0.01$, (c) $d_1 = 0.1$, (d) $d_1 = 1$ cases. The scale of z is three times larger than that of x.

3. Measurements of reflection curves of bent crystal using double crystal spectrometer

Note that a Gaussian distribution has been employed, so far for the rocking curve of a bent crystal, which for a perfect crystal, in particular, the deviation in terms of the width, the peak reflectivity and the shape, may be substantial. Several investigations have been performed to measure the reflection curves of bent crystals as well as their integrated reflectivities based upon the Takagi–Taupin theory of deformed crystal using both dispersive and non-dispersive double-crystal spectrometer geometries. The well-known expression of the reflected intensity $P(\beta)$ is shown in the following:

$$P(\beta) = \int\int\int G(\alpha,\phi)J(\lambda-\lambda_0)C_1\left[\Delta\theta_1 - (\lambda-\lambda_0)\frac{\partial}{\partial\lambda_0}\Theta(\lambda_0)\right] \times C_2\left[\pm\beta \mp \Delta\theta_2 - (\lambda-\lambda_0)\frac{\partial}{\partial\lambda_0}\Theta(\lambda_0)\right] \mathrm{d}\alpha\mathrm{d}\phi\mathrm{d}\lambda, \tag{6}$$

where C_1 and C_2, including the rocking curves $\Delta\theta$ and the angular deviation from the wavelength spread, are reflection curves for crystal 1 and 2, respectively. Note that $\Delta\theta$ are the same functions as in Eq. (2), but are expressed in angular coordinates in this case. In a dispersive setting, a flat and a bent crystal are used to form

an achromatic $(n, +n)$ arrangement shown in Fig. 9a. The flat crystal can be located in various positions between the bent crystal and the virtual source q′, since the dispersion of the flat crystal does not depend on the distance to the source. The theoretical rocking curve of the bent crystal can be calculated by using Eq. (6), and convolution with the flat crystal reflection curve as well as the source broadening due to the finite slit size. Rocking curves were measured reproducibly for a spherically bent crystal with bending radius, $R_1 = R_2 = 1$ in normalized coordinates (a solid line in Fig. 9b). The dashed line represents the calculated reflection curve of the bent crystal. The adequate agreement, especially for the asymptotic wing, confirms the reflection curve calculated by using the Takagi–Taupin theory.

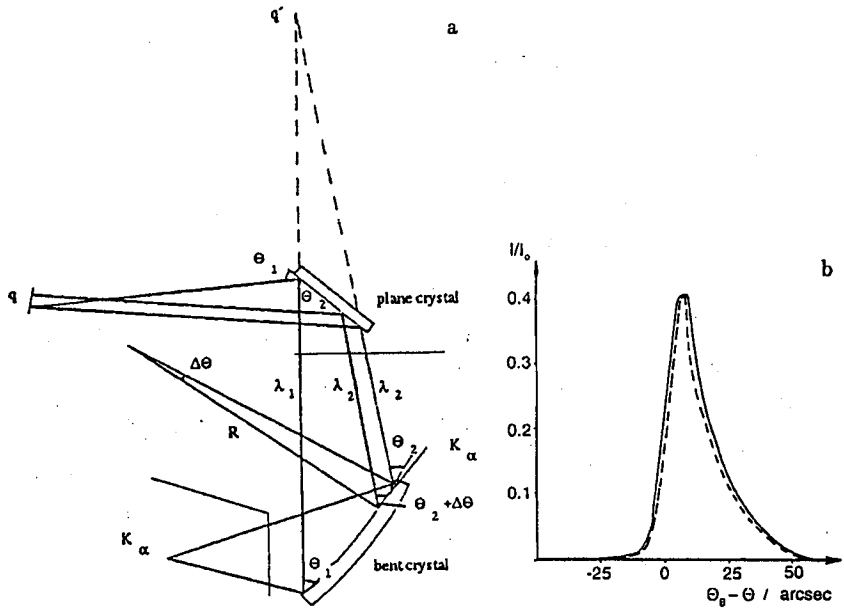

Fig. 9. Measurement of rocking curves using dispersive double-crystal spectrometer. (a) Experimental set-up for achromatic rocking curves of bent crystals, (b) measured rocking curve of a spherically bent crystal (R = 151.7 mm) (solid line) compared with the calculated reflection curve folded with the instrumentation function (dashed line).

Similarly, a non-dispersive setting of achromatic arrangement with a bent and a flat crystal was also devised to measure rocking curves of bent crystals. The experimental set-up is shown in Fig. 10a, and the $\Delta(\alpha_1 - \alpha_2)$ value was measured by changing the radius of the curvature, as well as rotating the bent crystal to find the smallest separation of the doublets, which is shown in Fig. 10b. Once, the optimal radius of curvature is determined, the rocking curve of the bent crystal can be measured by rotating the crystal in a non-dispersive fashion, in other words, the rocking curve is independent of the polychromaticity of the incident beam. The rocking curve of silicon (400) was obtained as shown in Fig. 10c. In this case, the advantage of using achromatic arrangement is evident since the diffracted X-ray intensity from the bent crystal consists of both K_{α_1} and K_{α_2} lines.

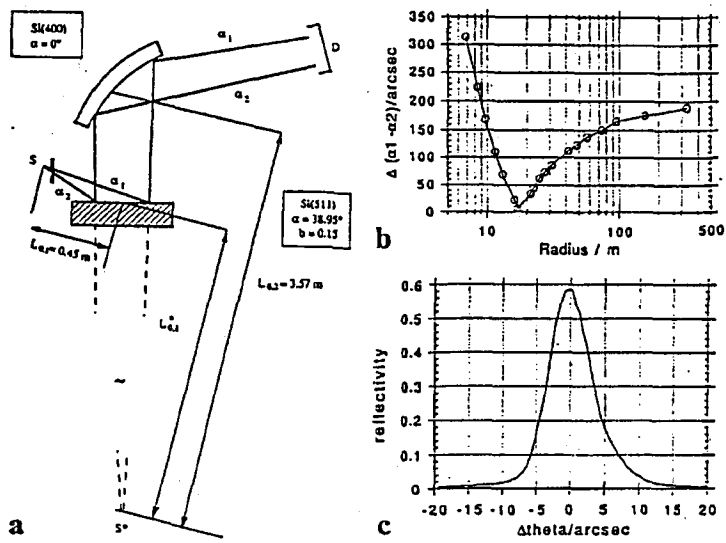

Fig. 10. Measurement of rocking curves using non-dispersive double-crystal spectrometer. (a) Experimental set-up; (b) Angular difference of K_{α_1} and K_{α_2} lines in dependence of the cylindrical radius of curvate; (c) Rocking curve of Si(400) ($R = 17.02$ m).

4. Crystal anisotropic effects of bent diffractors

In order to investigate the behavior of bent crystal, the anisotropic elasticity theory has been applied to singly and doubly bent crystals. Based on the pure bending model, the displacement vector u_y is expressed as the following:

$$u_y = -\frac{X^2}{2R_1} - \frac{Z^2}{2R_2} + \frac{3(s_{31}m_1 + s_{32}m_2)}{4t}, \tag{7a}$$

where

$$\frac{1}{R_1} = 12s_{11}\frac{m_1}{t^3} + 12s_{12}\frac{m_2}{t^3},$$

$$\frac{1}{R_2} = 12s_{21}\frac{m_1}{t^3} + 12s_{22}\frac{m_2}{t^3} \tag{7b}$$

are the characteristic radii of curvature in the meridional and sagittal planes. R_1 and R_2 are normalized and divided by $2R$, the diameter of the focal circle. m_1 and m_2 are bending moments applied in two orthogonal directions, t is the thickness of the crystal plate, and s_{ij} are the compliance tensor components. This displacement vector expression is similar to the surface equation used for deriving Eq. (2). The fundamental difference, however, is that the crystal anisotropic properties, in this case, are taken into account. This implies that the radius of curvature is not only a geometric quantity, but is the characteristic of the physical properties for a bent crystal. In cylindrical bending, instead of setting R_2 being infinity, (Table II) the effect of the anticlastic curvature in the direction perpendicular to the focal plane can be readily calculated from Eq. (7). The anticlastic curvature occurs when the

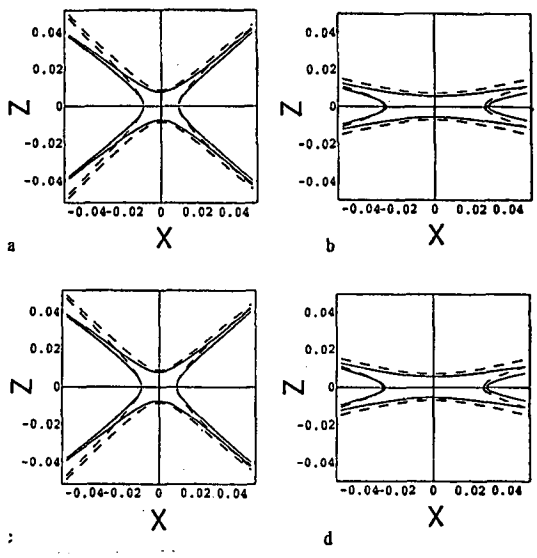

Fig. 11. Comparisons of diffracting regions for cylindrically bent crystal geometry with $\Delta\theta_0 = 10^{-4}$ radian between with anisotropic effects (case 1) and without anisotropic effects (case 2). (a) and (b) are the comparison of case 1 (solid line) and case 2 (dashed line) for a Si (200) at $\theta_B = 25°$ and 75°, respectively, and (c) and (d) are for a Si(111) at $\theta_B = 25°$ and 75°, respectively.

signs of R_1 and R_2 are opposite, in other words, the ratio of R_1 and R_2, which is determined by the values of s_{ij}, is negative.

For a given silicon crystal, the ratios of R_1/R_2 in the case of (200) and (111) reflections are calculated as -3.589 and -3.811, respectively. The anticlastic curvature occurs in both cases with similar values, which suggests that R_2 is insensitive to the crystal orientation. As an example, Fig. 11 illustrates the contours of the diffraction region on the crystal surfaces of (200) and (111) reflections for a cylindrically bent silicon crystal, which are compared to the case of $R_1 = 1$ and $R_2 = \infty$. In both cases, the narrowing of the diffraction region in the z direction are observed.

5. Linear dispersions of various diffraction geometries

For different focusing geometries, it is desirable to be able to calculate their linear dispersion analytically for a given radiation and a radius of curvature. The inverse of the linear dispersion, $(\mathrm{d}x/\mathrm{d}\lambda)^{-1}$, can be obtained as the following:

$$\frac{\mathrm{d}\lambda}{\mathrm{d}x} = \cot\theta_B \lambda \frac{\mathrm{d}\Delta\theta(x, z_0)}{\mathrm{d}x},$$
$$\frac{\mathrm{d}\lambda}{\mathrm{d}z} = \cot\theta_B \lambda \frac{\mathrm{d}\Delta\theta(x_0, z)}{\mathrm{d}z}. \tag{8}$$

The differentiation of $\Delta\theta$ with respect to x and z can be readily calculated from Eq. (2). For a given crystal and a perfect alignment, namely, $x_1 = y_1 = z_1 = 0$,

the resolution depends on the size of the diffractor, the bending radius, and the wavelength of the radiation. For the sake of the illustration, only the spherically bent crystal is calculated here. Using Tables I and II, Eq. (8) can be calculated as the following:

$$\frac{d\lambda}{dx} = \frac{\cot^2\theta_B\lambda}{2R}\left(x + \frac{3}{2}\cot\theta_B x^2 - \frac{\cot\theta_B z_0^2}{2}\right),$$

$$\frac{d\lambda}{dz} = \frac{\cot^3\theta_B\lambda}{2R}x_0 z, \tag{9}$$

where R is the radius of the focal circle, and x_0 and z_0 are constants. It can be seen that the linear dispersion in the plane of the focal circle, $dx/d\lambda$ increases, as θ_B becomes large, which is evident for the case of close to the normal incidence. The value of $d\lambda/dx$ is inversely proportional to the radius of curvature, which is consistent with the dispersion plane of the Johann geometry. If we let $z_0 = 0$, then the value of $d\lambda/dx$ is finite for a given value of x, which is, in fact, related to the rocking curve width. Evidently, the improvement of the linear dispersion can be achieved by limiting the size, or the diffracting region on the crystal surface, to the region where the intensity distribution is appreciable. It is more interesting to examine the term $d\lambda/dz$ in the direction perpendicular to the dispersion plane. If the value of x_0 is close to zero, then $d\lambda/dz$ tends to zero, in other words, the linear dispersion becomes very large. Certainly, this is an ideal case, since, in practice, it is difficult to locate the detector at the exact position of $x_0 = 0$ accurately. It is evident, however, that the dispersion in z direction is much larger than that in x direction. It should be cautioned that this conclusion is based upon the case where the crystal is perfectly aligned. If the misalignment parameters are non-zeros, then the value of $d\lambda/dz$ is finite, even when $x_0 = 0$.

6. Conclusions

A procedure for analytical calculations of X-ray intensity profiles on the bent crystals' surface and on the image plane is described. For various focusing geometries, it allows one, in general, to obtain analytical formulae for evaluating the shape, the width, and the peak of the intensity distribution. Moreover, it is demonstrated that this approach is applicable not only to a point source, but also a quasi-parallel X-ray beam, such as X-ray plasma sources and synchrotron radiation sources. Based upon the analytical formulae, it is possible to calculate linear dispersion quantitatively, the spectral and spatial resolutions for different bent crystal geometries, which is invaluable to various X-ray spectroscopic experiments.

The limitation of the procedure, however, is the assumption of the Gaussian distribution which contains no information of X-ray scattering process within the bent crystal. Using Takagi–Taupin dynamic theory of bent crystals and achromatic double crystal spectrometer, we have been able to measure reflection curves of bent crystals. As a result, the integrated reflectivities of the bent crystals may be calculated. The application of anisotropic elasticity theory to bent crystal provides the information of the anisotropic crystal behavior when a crystal is bent to a certain

form with respect to its orientation. It is demonstrated that using a pure bending model, the occurrence of the anticlastic curvature is a direct consequences of the anisotropic behavior of cylindrically bent crystals, which is accurately described by the theory presented here. For doubly curved crystals, a more practical model, e.g. large deflection, should be employed to take into account of the strain due to the stretching in the neutral bending axis.

References

[1] F.N. Chukhovskii, M. Krisch, *J. Appl. Cryst.* **25**, 211 (1992).

[2] W.Z. Chang, D.B. Wittry, *J. Appl. Phys.* **74**, 2999 (1993).

[3] E. Förster, K. Gäbel, I. Uschmann, *Rev. Sci. Instrum.* **63**, 5012 (1992).

[4] F.N. Chukhovskii, M. Krisch, A.K. Freund, *Rev. Sci. Instrum.* **63**, 920 (1992).

[5] I. Uschmann, E. Förster, K. Gabel, G. Holzer, M. Ensslen, *J. Appl. Cryst.* **26**, 405 (1993).

[6] F.N. Chukhovskii, W.Z. Chang, E. Förster, submitted to *J. Appl. Cryst.* (1994).